

ments. A fair quality scope of the rolling ratio is calculated based on comparison and observational validation.

To simulate the non-linear problem that characterizes the ring rolling process, finite element codes are available [4]. The analysis is done using ANSYS. The parameters including speed, axial roller feed, and driving rollers were analyzed from the study [5]. The optimal relationship between the process parameters is identified from the analysis. The stress and strain values are generated at different speeds. Critical and failure values are also obtained. The research was carried out for structural steel and aluminum as the workpiece, taking the characteristics of the metal into the account [6].

3 Research Methodology

3.1 Process of ring rolling

The design scheme of the ring rolling process is presented in Figure 1.

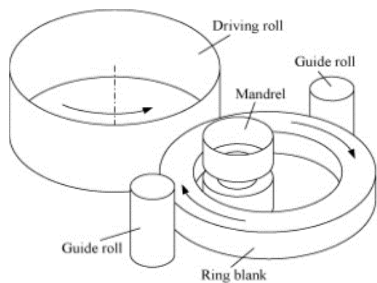


Figure 1 – The ring rolling process

Two rollers that rotate in the opposite direction are fed in the ring rolling material. The gap between the rollers is lower than the material thickness caused by deformation. It is caused to elongate due to reduced material thickness. Material-roller resistance induced the material to move [2]. The volume of deformation in a single pass is limited by roller friction. If the thickness varies, rollers can be slipped. Certain procedures such as shearing, flattening and punching are to be completed before the ring rolling process in order to generate the final product. Shearing is the method of removing a necessary blank from the stock. Flattening is a method of adding sufficient force to reduce the height of the original element [5]. Eventually, the punch and dies design creates a gap in the part [7]. The processing of ring rolling is given in Figure 2

3.2 Typical Ring Rolling Products

Rolled rings find application in bearings, slewing bearings, turbine disks and gear blanks [8]. Ring rolling machines are also used in producing solid wheels and wheel disks for high-speed trains, locomotives, railway carriages, trams, and subway trains. More examples of the varied uses of ring rolling items includes bevel gear and axle drive wheels for the automotive industry, transmission manufacturing, turbine manufacturing (turbine disks for plane propulsion engines), flanges in the computer and plant construction industry, rings for tower flanges (in off-shore wind turbines) and roller bearings (cold spinning) [9].

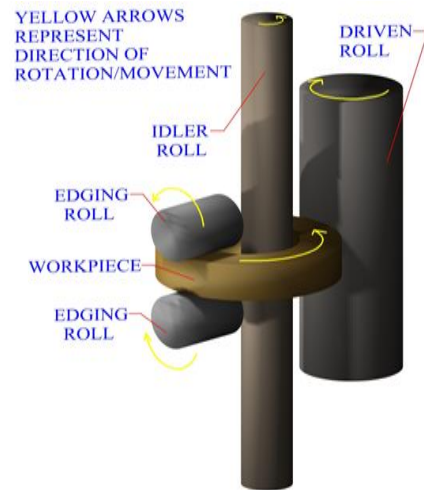


Figure 2 – The process of ring rolling

3.3 Analytical description of ring rolling

Kalpak Jian and Schmidt's flat rolling analysis is extended to the process of ring rolling [9]. Process parameters are defined as given in Figure 3.

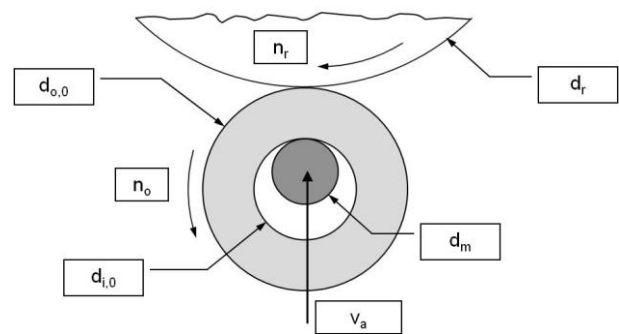


Figure 3 – Description of the ring rolling process

The parameters used in the analysis are d_i – inner diameter; d_o – outer diameter; d_r – roll diameter; d_m – mandrel diameter; n_r – roller rotational speed; n_o – ring rotational speed; v_a – advance velocity of the mandrel.

The first relationship to be developed is the dependency by volume preservation between cross-sectional thickness and diameter. The plain strain is presumed in this situation, therefore there is no strain in the width direction.

The main geometric dependencies are based on the following requirement of the constant volume:

$$\begin{aligned} \pi(d_o^2 - d_i^2)w/4 &= \pi(d_{o,0}^2 - d_{i,0}^2)w/4; \\ d_i &= [d_o^2 - (d_{o,0}^2 - d_{i,0}^2)]^{1/2}. \end{aligned} \quad (1)$$

Therefore, the internal diameter relies on the external diameter and the actual empty volume as determined from the initial measurements of the circle. The next step in the analysis is to provide equivalence to the process of flat rolling by equating the contact lengths between the material and the roll or mandrel. This analysis targets defining the equivalent diameter of a flat rolling process roll to represent the more complex curvilinear ring roll.

A result for the forming roll which undergoes convex-convex contact is given by

$$d_{r,eq} = d_r/[1 + 2d_r/(d_{o,0} + d_o)]. \quad (2)$$

Therefore, the corresponding flat rolling size is less than the true diameter of the greater convex-convex touch roll. Similarly, the diameter of a mandrel is given by

$$d_{m,eq} = d_m/[1 - 2d_m/(d_{i,0} + d_i)]. \quad (3)$$

The conversion of the convex-concave touch of the mandrel to the inner ring surface leads the corresponding flat roll size to increase than convex-flat contact for plain rolling. Now that the rolling phase of the circle has been converted into flat rolling, the draft issue needs to be addressed [10]. The draft is defined as the reduction of rolling height. The initial and final heights were independent of the rolling system itself for flat rolling. In-ring rolling, though, the heights of entry and exit are combined as the height of exit in one rotation becomes the height of entry for the next rotation. This coupling effect can be given in terms of the advance mandrel speed and the system's rotational speed [11]. When we consider the advanced instantaneous velocity $v_a = d_h/d_t$, and if the velocity of the mandrel is unchanged, the height shift in a single revolution can be interpreted as a finite difference $v_a = (h_1 - h_2)/t_r$, the period for a single rotation is determined from the ring and roll size and rotational velocity: $t_r = 60/n_{o,1} = 60\pi d/v_1 \approx 60\pi d/n_r = 60d_o/(d_r n_r)$.

Therefore, the height change can be described as

$$h_1 - h_2 = 60d_0 v_a / (d_r n_r). \quad (4)$$

The h_1 and h_2 reflect the heights inside and outside the rolling area and the stress applied to the ring segment is proportional to the original sectional size, as there is no rotational annealing process. When we consider the peak draft state as the point of equilibrium of frictional and natural forces in the direction of rolling, a total approval angle for flat rolling can be given [12]. This condition is shown in Figure 4, where F_n describes the normal force against the piece of work and F_f the tangential frictional force to the move.

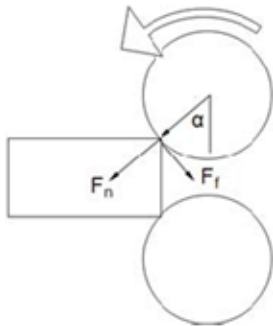


Figure 4 – Force balancing at critical rolling height

The following force component constraint must be considered in order to pull the material into the process:

$$\begin{aligned} F_f \cos\alpha &> F_n \sin\alpha; \\ F_f &= \mu F_n > F_n \tan\alpha; \\ \mu &> \tan\alpha. \end{aligned} \quad (5)$$

If we assume that the rolling radius exceeds the change in height (large rolling assumption),

$$\tan\alpha \approx \sin\alpha \approx (\Delta h/R)^{1/2}; \Delta h_{max} = \mu^2 R. \quad (6)$$

This analysis is summarized in [4]. Setting these maximum drafts in the following relationship

$$\begin{aligned} \Delta h_{max} &= \mu^2 d_r / 2 = 60d_0 v_a^{max} / (d_r n_r); \\ v_a^{max} &= \mu^2 d_r^2 n_r / (120d_0). \end{aligned} \quad (7)$$

Therefore, to maintain the rotation of the ring during rolling, an upper limit is established on the prescribed mandrel advance velocity [2].

3.4 Numerical simulation

Figure 6 describes the modeling of ring rolling that includes workpiece, mandrel, and roller guide. Modeling is done using solids works and the mesh analysis is done in ANSYS. Wire modeling and meshing of ring rolling are given in Figure 5. The mesh domain is created for quality analysis.

Finite Element Analysis (FEA) is performed using the FEA software package called ANSYS. The computer package introduces and solves the formulas that control the action of elements. The material used for the process is Aluminum 6061 alloy [12]. The material properties are provided in Table 1.

The pressure of the roller against the workpiece could be either increased or decreased, based on the desired shape of the workpiece [8].

The roller moves around the workpiece that is fixed at the stationary state. The rotational speed of the roller is 40 rad/sec to get the desired dimensional output of the workpiece.

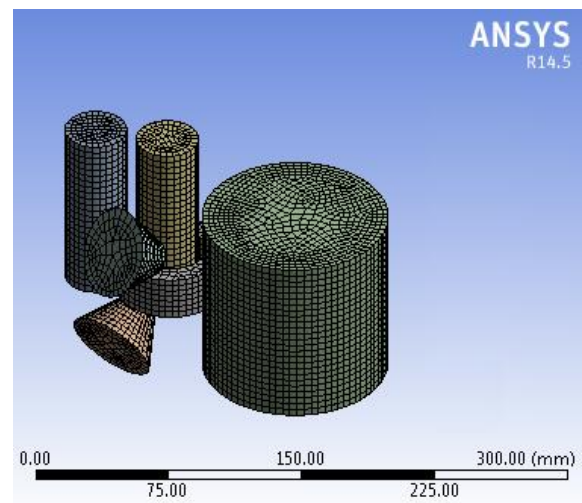


Figure 5 – The meshing of the ring rolling process

Table 1 – Properties of Aluminum 6061 alloy

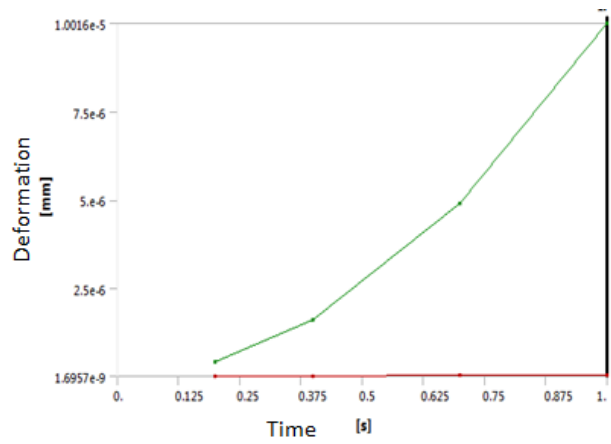
Density, kg/m ³	2700
Brinell's hardness	95
Rockwell hardness	40
Tangent modulus, MPa	1330
Ultimate tensile strength, MPa	310
Tensile yield strength, MPa	276
Young's modulus, MPa	68.9
Ultimate bearing strength, MPa	607
Bearing yield strength, MPa	386
Poisson's ratio	0.33
Fatigue strength, MPa	96.5
Shear modulus, MPa	26
Shear strength, MPa	207
Specific heat capacity, J/(kg·K)	896
Thermal conductivity, W/(m·K)	167
Elongation at break, %	12

4 Results

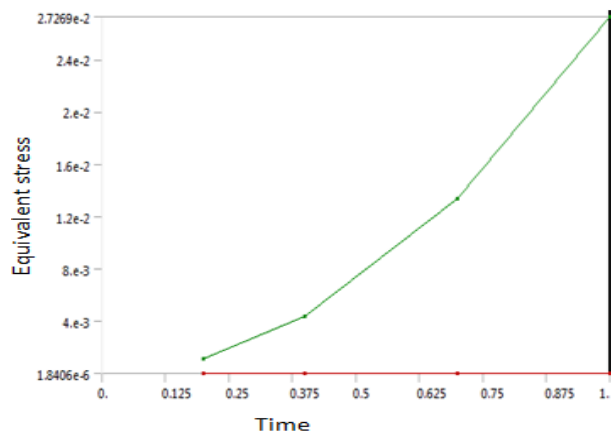
Rotational velocity is directly proportional to the time, which means that when the velocity is increasing the time taken for the process increases linearly. In this case, the rotational acceleration is equal to 50 rad/s².

From Figure 6 a, it can be observed that the maximum and minimum static structural deformations for the process are 5.96 nm. Figure 6 b describes the maximum static structural equivalent stresses equal to 0.027 MPa.

Figure 7 a, b describes that deformations and stress increase with an increase in time. It can be observed from Figure 8 that the maximum static structural normal stress for the process is equal to 19.8 kPa.

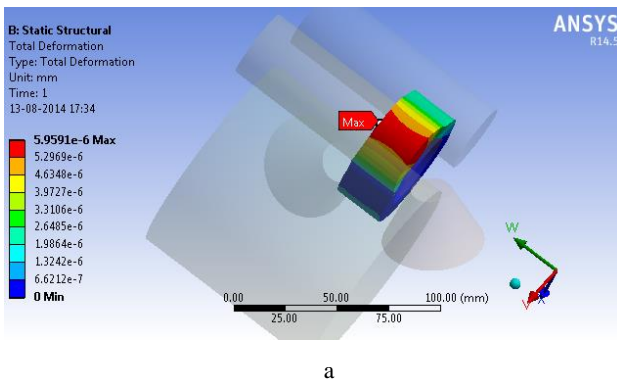


a

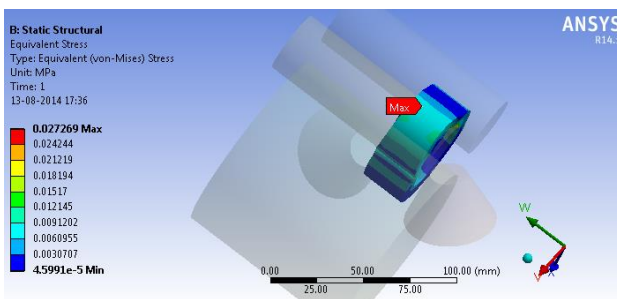


b

Figure 7 – The maximum values of deformations (a) and equivalent stresses (b) in time



a



b

Figure 6 – Total deformations (a) and von Mises equivalent stresses (b)

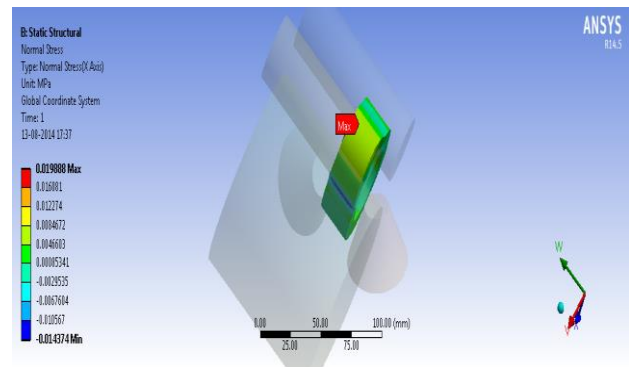


Figure 8 – Normal stresses

5 Conclusions

The finite element analysis is done by considering aluminum 6061 alloys as workpiece material and structural steel as roller material in the ring rolling process. The values of normal stress, von Mises stresses, and strain energy are obtained. Fatigue power, mandrel life is accomplished by considering the number of cycles it could withstand. From the analysis, it is observed that von Mises stress of the work material is below the actual values. Workpiece strength is determined by changing the velocity of idle role and workpiece.

References

1. Banerjee, P., Huir, N. B. (2019). Finite element modeling of ring rolling process. *Materials Today: Proceedings*, Vol. 11, pp. 843–848.
2. Yang, H., Guo, L., Zhan, M., Sun, Z. (2006). Research on the influence of material properties on cold ring rolling processes by 3D-FE numerical simulation. *Journal of Materials Processing Technology*, Vol. 177, pp. 634–638.
3. Allegri, G., Giorleo, L., Ceretti, E., Giardini, C. (2017). Driver roll speed influence in ring rolling process. *Procedia Engineering*, Vol. 207, pp. 1230–1235.
4. Guillaume, C. and Brosius, A., 2019. Simulation methods for skew rolling. *Procedia Manufacturing*, 27, pp.1-6.
5. Dandagwhal, R. D., Kalyankar, V. D. (2019). Design optimization of rolling element bearings using advanced optimization technique. *Arabian Journal for Science and Engineering*, pp. 1–16.
6. Tripathi, A., Medhavi, A. (2014). Finite element simulation of hot rolling for an aluminum 2024 plate. *International Journal of Scientific and Research Publications*, Vol. 4(12), pp. 361–365.
7. Allegri, G., Giorleo, L., Ceretti, E. (2019). Roll gap per rotation optimization in a radial ring rolling process. *AIP Conference Proceedings*, Vol. 2113(1), article number 040008.
8. Hua, L., Deng, J., Qian, D. (2017). Recent development of ring rolling theory and technique. *International Journal of Materials and Product Technology*, Vol. 54(1-3), pp. 65–87.
9. Quagliato, L., Berti, G. A. (2016). Mathematical definition of the 3D strain field of the ring in the radial-axial ring rolling process. *International Journal of Mechanical Sciences*, Vol. 115, pp. 746–759.
10. Sun, B., Xu, J., Xing, C. (2019). Numerical and experimental investigations on the effect of mandrel feeding speed for high-speed rail bearing inner ring. *The International Journal of Advanced Manufacturing Technology*, Vol. 100(5-8), pp. 1993–2006.
11. Meng, W., Zhao, G. Q. (2014). Effects of key simulation parameters on conical ring rolling process. *Procedia Engineering*, Vol. 81, pp. 286–291.
12. Wu, Q., Wu, J., Zhang, Y. D., Gao, H. J., Hui, D. (2019). Analysis and homogenization of residual stress in aerospace ring rolling process of 2219 aluminum alloy using thermal stress relief method. *International Journal of Mechanical Sciences*, Vol. 157, pp. 111–118.
13. Wasa, N., Fukui, T. (2019). *Ring Rolling Mill and Method for Manufacturing Ring Rolled Material*. U.S. Patent Application 10/286,443.
14. Yagami, T., Teramae, T., Fujita, E., Nagao, S., Mukouse, R., Iwasa, N., Fukui, T., Aoki, C. (2018). *Material for Ring Rolling*. U.S. Patent 10,094,238.

УДК 624.014

Моделювання та оптимізаційний розрахунок процесу прокатування кілець з конструкційної сталі та алюмінієвого сплаву

Тя П. С., Кумар М. Д., Крішна Р., Срінівасан М.

Інститут технологій та наук ім. Пейс, 523 272, м. Онголе, Індія

Анотація. Поточні дослідження проводилися за допомогою програмного комплексу ANSYS для оптимізації параметрів процесу прокатування кілець. Для оптимізації процесу прокатування були оцінені такі параметри, як швидкість, осьова подача ролика і параметри приводних роликів. Як підхід до оптимізації процесу було оцінено оптимальні значення параметрів та взаємозв'язки між ними. Параметри напружено-деформованого стану оцінювались для різних швидкостей і сил, а також визначались відповідні значення критичних параметрів. Для проведення дослідження було обрано конструкційні сталі та алюмінієві сплави, оскільки саме вони використовуються для виготовлення функціональних елементів і деталей коліс. Дослідження проводилось шляхом зміни кутової швидкості направляючого ролика у діапазоні від 40 до 45 рад/с і зміни кутової швидкості деталі у діапазоні від 200 до 250 рад/с. Крім цього, втомна міцність робочих частин пристрою визначалася на основі аналізу кількості циклів навантаження до відмови. Також було проаналізовано напруження і пластичні деформації.

Ключові слова: валик, ANSYS, заготовка, пластичні деформації, еквівалентне напруження за Губером-Мізесом-Генки, металевий сплав.